Journal of Radioanalytical and Nuclear Chemistry
https://doi.org/10.1007/s10967-025-10153-8

# Radiogenic heat production and its contribution to terrestrial heat flow in the eastern Ordos Basin

Xiaoxue Jiang[1,2] · Chuanqing Zhu[1,2] · Lu Luo[3,4] · Shaochuan Sun[3,4] · Dan Li[3,4] · Keting Fan[1,2] · Fang Xie[1,2] · Yuanjin Sun[1,2]

Received: 19 December 2024 / Accepted: 21 April 2025


**Abstract**
The heat generation rates of 6572 rock samples from 26 boreholes in the eastern Ordos Basin are calculated and compared with measured values using gamma ray logs and gamma ray spectrometry logs. Results show that calculations using natural gamma spectrum logging are more accurate. The average heat production values for different lithologies are as follows: sandstone $1.55 \pm 0.68$ μW/m$^3$, siltstone $1.68 \pm 0.41$ μW/m$^3$, mudstone $2.05 \pm 0.70$ μW/m$^3$, limestone $0.51 \pm 0.48$ μW/m$^3$, dolomite $0.40 \pm 0.26$ μW/m$^3$, salt gypsum $0.27 \pm 0.18$ μW/m$^3$. The heat production in the sedimentary layers of the eastern Ordos Basin ranges from 1.37 to 3.45 mW/m$^2$, offering valuable insights into the lithospheric thermal structure.

**Keywords** Gamma ray spectrometry logs · Radiogenic heat production · Heat flow contribution · Ordos Basin

## Introduction

Containing over 60 heat-producing unstable nuclides, Rocks are a primary heat source in the Earth's interior [1, 2]. Among these, uranium (U), thorium (Th), and potassium (K) dominate, with their distribution significantly influencing the Earth's internal temperature [3, 4]. Radiogenic heat from these elements contributes 30–50% of terrestrial heat flow. The radioactive radiogenic heat production rate, defined as the energy released per unit volume of rock through decay, is a critical parameter for understanding geothermal fields and the thermal evolution of lithosphere [5–8]. Three primary methods are used to determine radioactive radiogenic heat production rates. The first involves direct measurement of U, Th, and K concentrations using techniques like ICP-MS and XRF, which yield precise data but are costly [9, 10]. The second estimates heat generation from seismic wave velocities, though this method is less accurate [11]. The third, natural radioactive logging, measures U, Th, and K concentrations in situ, offering high-quality data at a lower cost while addressing limitations of the other methods [5, 12]. The Ordos Basin, located in the western part of the North China Craton, is a typical stable craton basin with abundant oil, gas, coal, metal, and geothermal resources. While numerous studies have been conducted on the basin's heat flow distribution, current geothermal field, and tectonic thermal evolution, systematic research on the characteristics of radioactive heat generation in the sedimentary layers remains insufficient. This is especially apparent in the eastern part of the Ordos Basin, where heat flow values are higher compared to other regions. The lack of basic thermal property parameters in this region limits the simulation of the regional geothermal field and hinders a deeper understanding of the genetic mechanisms underlying the geothermal system. Therefore, analyzing the radioactive heat production rate in the eastern region is of great significance [13, 14]. This study calculates radioactive radiogenic heat production rates using natural radioactive logging data from 26 wells in the eastern margin of the Ordos Basin. A representative radiogenic heat production rate profile is developed, analyzing the concentrations of heat-producing elements, their contributions to heat production, and radiogenic heat production rates of various rock types. The impact of radiogenic element variability

✉ Chuanqing Zhu
zhucq@cup.edu.cn

1 State Key Laboratory of Deep Geothermal Resources, China University of Petroleum (Beijing), Beijing 102249, China

2 College of Geosciences, China University of Petroleum (Beijing), Beijing 102249, China

3 State Key Laboratory of Deep Geothermal Resources, Beijing 100083, China

4 SINOPEC Star Petroleum Corporation Limited, Beijing 100083, China

Published online: 26 May 2025

on heat generation is also assessed, providing insights into geothermal systems and contributing to understanding the lithosphere's thermal structure in the eastern Ordos Basin.

## Geological Background

The Ordos Basin, located on the western margin of the North China Plate, is divided into six tectonic units based on its evolutionary history: Yimeng Uplift, Weibei Uplift, Jinxi Flexural Fold Belt, Yishan Slope, Tianhuan Depression, and the Western Margin Buffer Zone [12] (Fig. 1). The study area, situated in the eastern part of the basin, has a basement composed of Archean and Lower Proterozoic metamorphic rocks, overlain by Paleozoic strata, including Cambrian, Ordovician, Carboniferous, and Permian formations. The sedimentary environment transitioned from marine carbonate deposition to terrestrial fluvial-delta systems [15, 16]. In the Cambrian and Ordovician periods, carbonate rocks dominate the lithology [17]. The Carboniferous Benxi Formation consists primarily of carbonate rocks, mudstone, and fine sandstone. The Taiyuan Formation, composed of epicontinental marine deposits, features a sequence of carbonate and clastic rocks [18]. The Permian Shanxi Formation represents a transition from marine to continental deposition, characterized by medium- to coarse-grained sandstone, siltstone, mudstone, and coal [19]. The Lower Shihezi Formation is primarily a delta plain deposit, with the upper section dominated by clastic sandstone and the lower section comprising fine-grained sandstone interbedded with shale. The overlying Upper Shihezi Formation consists mainly of mudstone. In the Shiqianfeng Formation, the sedimentary environment fully transitions to continental fluvial deposits, with lithology dominated by clastic rocks interbedded with purple-red sandstone and mudstone [20, 21].

## Materials and Methods

### Natural gamma ray and natural gamma spectrum logging

Gamma logging, one of the most widely used radioactive logging methods, measures the count rate or standardized readings of gamma photons with energies exceeding 100 keV. This technique indicates the total radionuclide content within the formation but is unable to distinguish between specific radionuclides. The radioactivity of rocks primarily depends on the concentrations of three radioactive

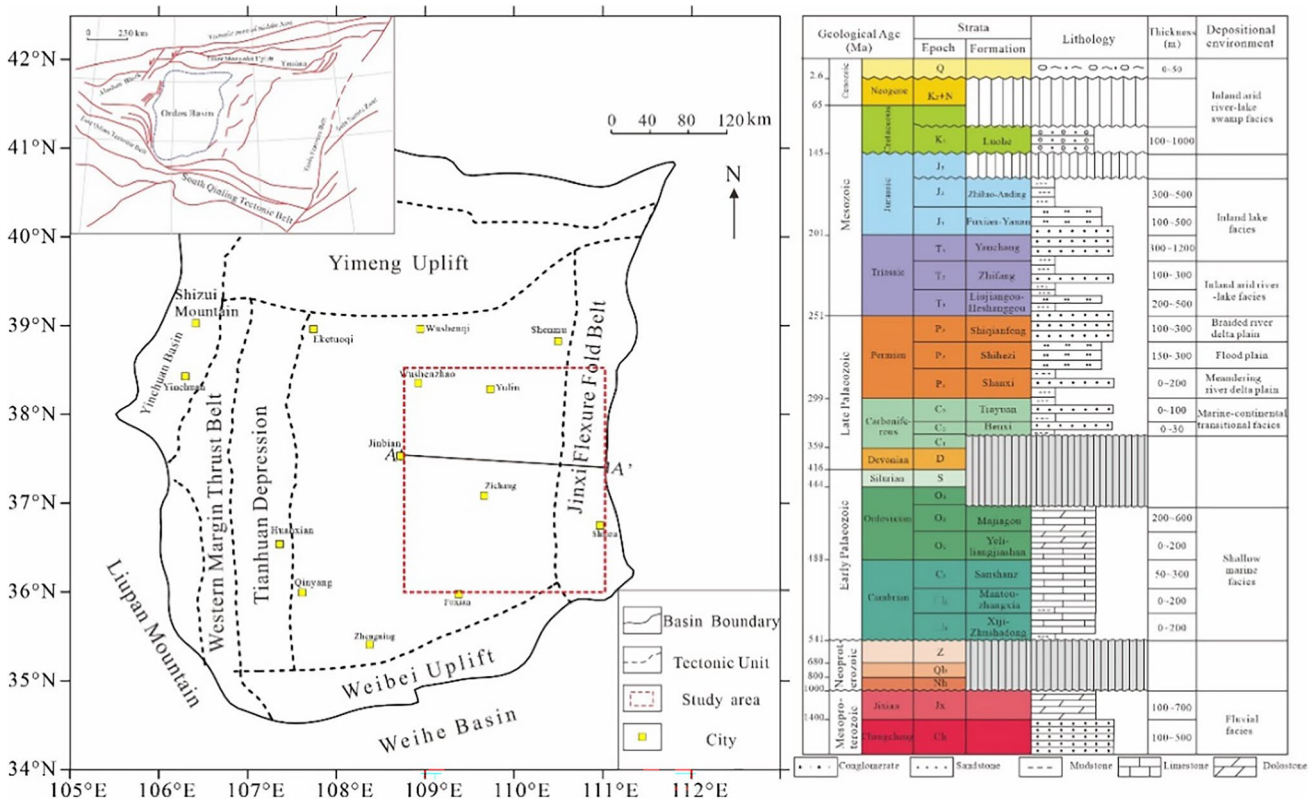


**Fig. 1** Tectonic division in the study area and integrated stratigraphic column

isotopes: uranium ($^{238}$U), thorium ($^{232}$Th), and potassium ($^{40}$K), each of which emits gamma rays with distinct characteristic energies.

Natural gamma ray spectrum logging refines this process by analyzing the gamma-ray spectrum to quantitatively assess the energy emitted by individual radioactive elements. This method enables the determination of their concentrations within the formation [22, 23].

## Calculation Methods

The radioactive radiogenic heat production rate of a rock represents the energy released per unit time due to the decay of radioactive elements within a unit volume of the rock [6]. The concentrations of uranium ($^{238}$U), thorium ($^{232}$Th), and potassium ($^{40}$K) at various depths can be determined from the natural gamma spectrum logging curve. When combined with the density logging data, the empirical formula proposed by Rybach is applied to calculate the radiogenic heat production rate at different depths. the formula is as follows [24]:

$$A = \rho\left(3.48 \times \left(C_K\right) + 2.56 \times \left(C_{Th}\right) + 9.52 \times \left(C_U\right)\right) \times 10^{-2} \quad (1)$$

in Eq. (1), $A$ represents the rock heat production rate in $\mu W/m^3$; $\rho$ is the rock density in $g/cm^3$; $C_K$ is the content of the K element in the rock (%); $C_{Th}$ is the content of the Th element in the rock, $10^{-6}$; and $C_U$ is the content of the U element in the rock, $10^{-6}$.

Gamma logging records the total gamma intensity from U, Th, and K in the formation. The sensitivity of the gamma logging tool to U, Th, and K is proportional to the corresponding radiogenic heat production rates in Eq. (1). Moreover, the ratio of Th/U and K/U in crustal rocks is generally constant. Therefore, within a specific interval of drilling depth, there exists a simple linear relationship between the gamma ray log counts and the radiogenic heat production rate. In 1986, Rybach proposed the GR-A(Gamma Ray—Radiogenic heat production rate) linear relationship by comparing measured radiogenic heat production rates with natural gamma counts, as shown in Eq. (2) [11]:

$$A = 0.0145[\mathrm{GR(API)} - 5.0] \quad (2)$$

This study collects natural gamma and natural gamma energy spectrum logging curves ($C_U$, $C_{Th}$, $C_K$) from 26 wells in the eastern Ordos Basin, with all logs measured at 0.125 m intervals. Figure 2 presents the heat generation rate results calculated using Eqs. (1) and (2), respectively. Equation (1) is applied to data from the natural gamma energy spectrum logging curve, which provides concentrations of uranium (U), thorium (Th), and potassium (K). Equation (2) is used for the conventional natural gamma logging curve, which reflects total gamma-ray intensity without resolving individual radionuclides. While the overall trends of the two methods are consistent, there are noticeable differences in the calculated values. Specifically, values derived using Eq. (1) are generally higher than those calculated using Eq. (2), especially in lithological intervals with high heat generation, such as the mudstone section from 3280 to 3360 m. In contrast, in low heat-generating sections, such as the sandstone interval from 2780 to 2860 m, the difference between the two methods is relatively small. To optimize data analysis while ensuring accuracy, one value in every thirty radiogenic heat production rate measurements, corresponding to 3.75-m intervals, was selected from the natural gamma spectrum log. Using Eqs. (1) and (2), radiogenic heat production rates for 6572 rock samples from 26 wells were calculated. A statistical comparison between the calculated and measured radiogenic heat production rates in the study area shows that the 6572 values derived from natural gamma spectrometry are closely aligned with the average and standard deviation of 59 measured radiogenic heat production rates. Specifically, the calculated average is $1.489 \pm 0.903$ $\mu W/m^3$, while the measured average is $1.568 \pm 1.192$ $\mu W/m^3$ [25–28] (Table 1). A comparison of radiogenic heat production rates calculated using different methods across various lithologies reveals the following: for sandstone, the average radiogenic heat production rate from the natural gamma log is $1.33 \pm 0.49$ $\mu W/m^3$, compared to $1.55 \pm 0.66$ $\mu W/m^3$ from the natural gamma spectrum log. The average measured rate for sandstone is $1.51 \pm 1.03$ $\mu W/m^3$. For mudstone, the average rates are $1.75 \pm 0.50$ $\mu W/m^3$ from the gamma ray log, $2.05 \pm 0.09$ $\mu W/m^3$ from the gamma ray spectrum log, and $2.22 \pm 0.78$ $\mu W/m^3$ from the measured data. For limestone, the average rates are $0.38 \pm 0.31$ $\mu W/m^3$ from the gamma ray log, $0.51 \pm 0.48$ $\mu W/m^3$ from the gamma ray spectrum log, and $0.40 \pm 0.21$ $\mu W/m^3$ from the measured data. While the differences in radiogenic heat production rates derived from various methods are relatively small, values calculated from the natural gamma spectrum log generally align more closely with measured values. Thus, the natural gamma spectrum logging method seems more suitable for this study area. However, as shown in Table 1, the average radiogenic heat production rates from both the gamma ray log and the natural gamma spectrum log tends to be lower than the measured averages. This discrepancy may arise from the limited number of salt samples in the 59 measured rock samples, as the logging curve calculations likely include a higher proportion of salt samples, which could affect the results.

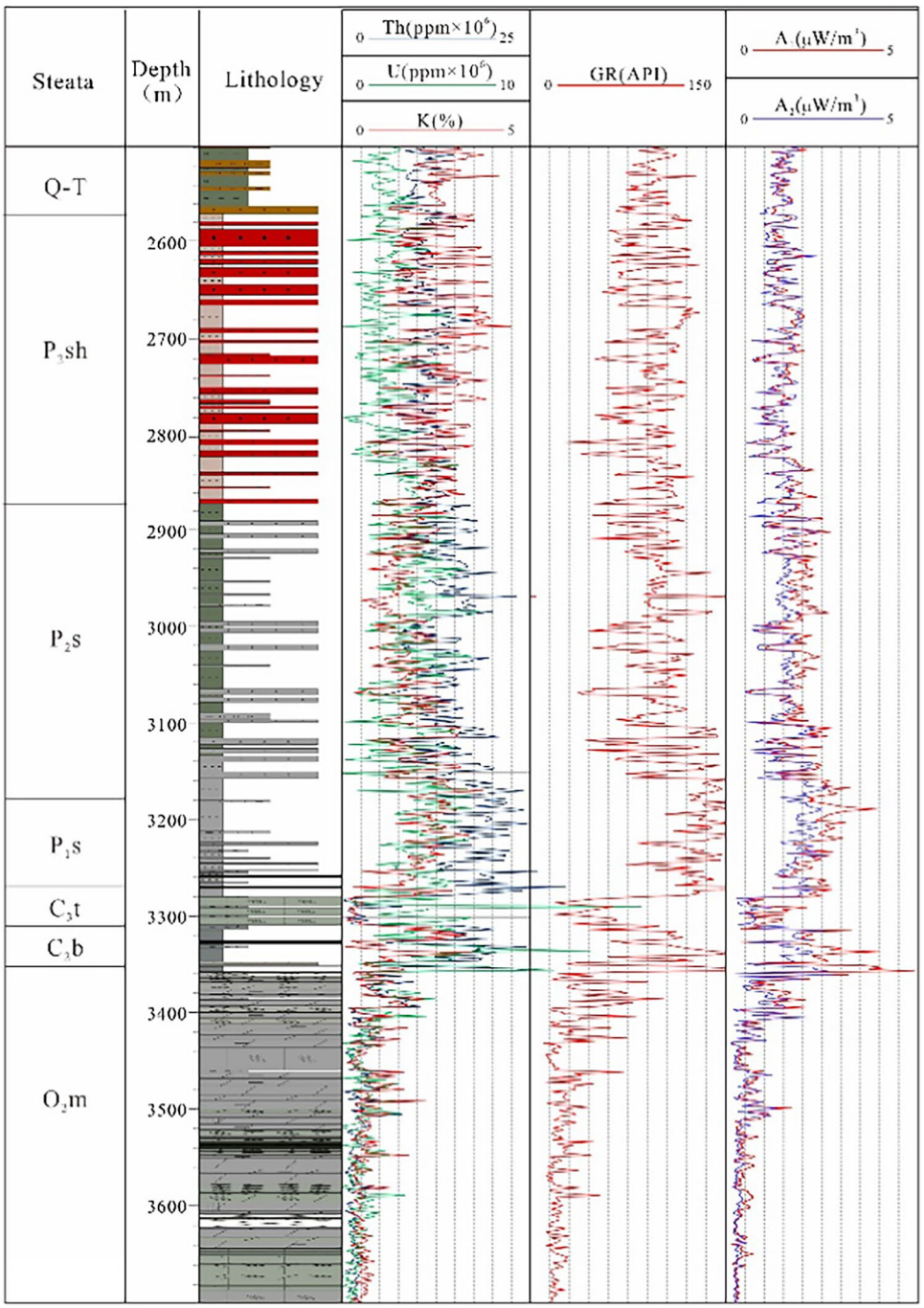


**Fig. 2** Gamma spectrum log, gamma log and calculated heat generation curves (2570–3720 m) for Well J05 in the Ordos Basin (A1: gamma spectrum log calculation results; A2: gamma Ray Log Calculation Results)

**Table 1** Comparison of calculated and measured radioactive radiogenic heat production rates from different logging Curves

| Method | Calculated (gamma ray log) | Calculated (gamma ray spectrum log) | Measured value [25–28] |
|---|---|---|---|
| Average (μW/m$^3$) | 1.268 | 1.489 | 1.568 |
| Standard Deviation (μW/m$^3$) | 0.710 | 0.903 | 1.192 |

## Results

The 6572 radiogenic heat production rate data points, obtained using the natural gamma spectrum curve, were primarily distributed between 0 and 2.5 μW/m$^3$, and their distribution pattern closely resembled that of the 59 measured radiogenic heat production rates (Fig. 3). The average radiogenic heat production rate of rocks in the eastern Ordos Basin is 1.489 ± 0.903 μW/m$^3$, which is lower than the average for the broader Ordos Basin. As shown in Fig. 4, the radiogenic heat production rates of typical wells in the study area vary, with the statistical results presented in Table 2. As shown in Fig. 4 and Table 2, the radiogenic heat production rates of rocks in the study area are generally higher in the Permian and Carboniferous formations and lower in the Ordovician formation. Furthermore, the distribution of radiogenic heat production rates varies significantly across different lithologies, indicating a strong lithological influence on heat production. For gypsum and salt rock samples, the radiogenic heat production rates are typically below 1.5 μW/m$^3$, with 84% of salt samples and

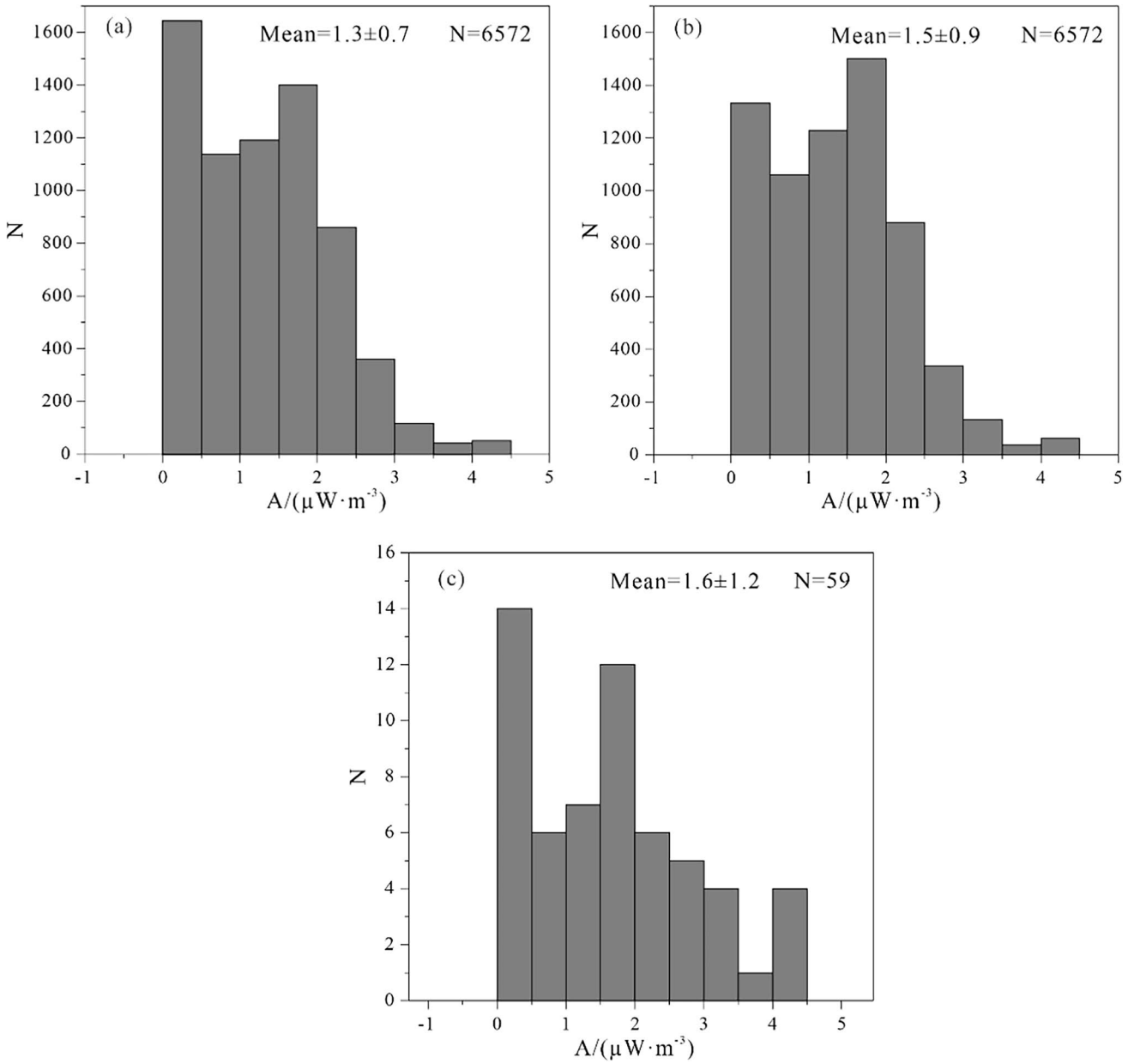


**Fig. 3** Statistical histograms of radiogenic heat production rates in the eastern Ordos Basin derived from: (a) gamma-ray spectrometry logs, (b) conventional gamma-ray logs, and (c) measured values

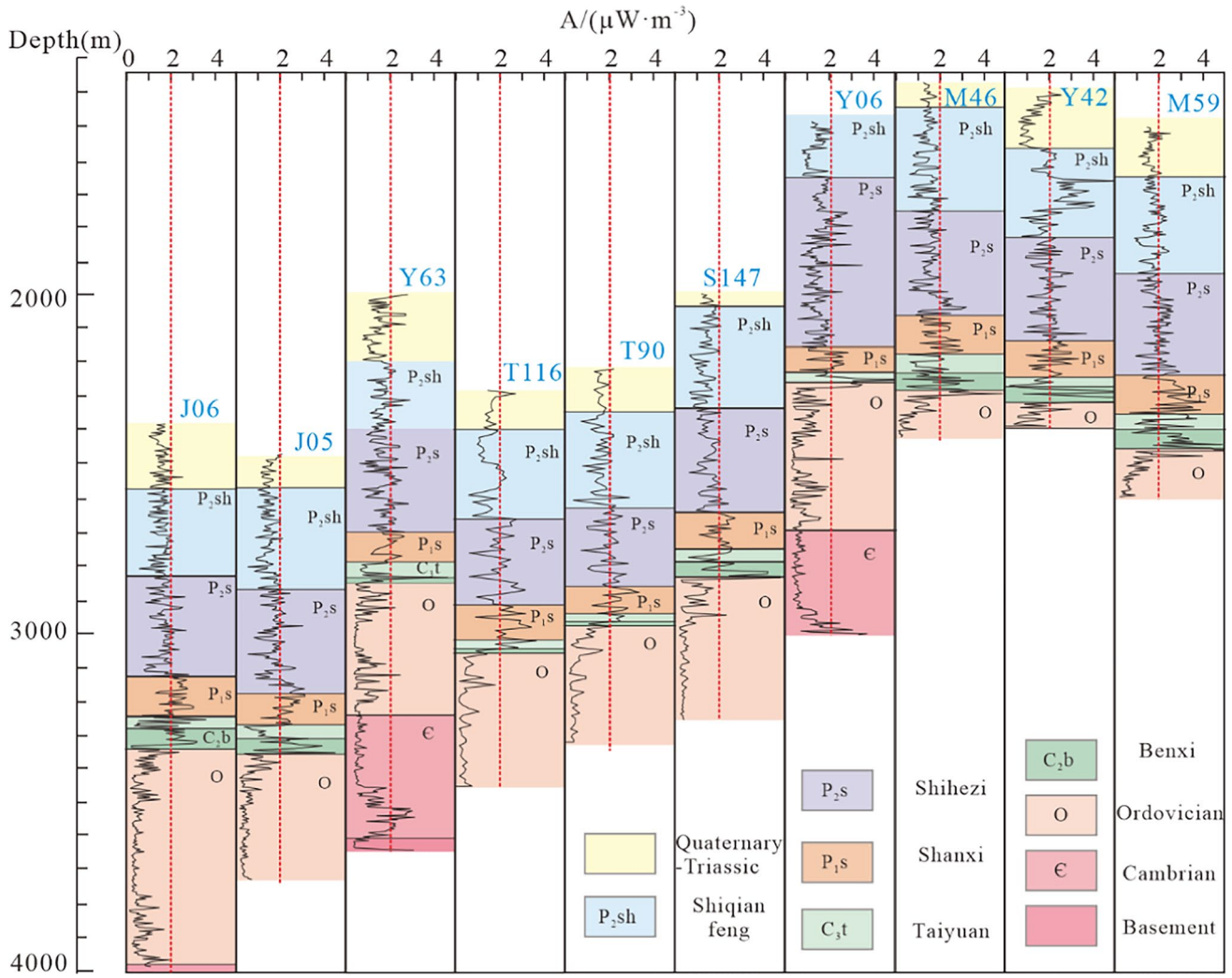


**Fig. 4** Variation of radiogenic heat production rates with depth for representative drilling lithologies in the eastern Ordos Basin

48% of gypsum samples having values lower than 0.5 μW/m$^3$. The radiogenic heat production rates in mudstone samples are more scattered; however, 85% of these samples exceed 1.5 μW/m$^3$, and 86% exceed 1.0 μW/m$^3$. In contrast, 61% of limestone samples have radiogenic heat production rates below 0.5 μW/m$^3$, with 87% falling below 1.0 μW/m$^3$. Most siltstone samples show radiogenic heat production rates between 1.0 and 2.5 μW/m$^3$, while sandstone samples are predominantly concentrated in the 1.0–2.0 μW/m$^3$ range.

## Discussion

### Radioactive heat generation of sedimentary and metamorphic rocks in the eastern ordos basin

The radiogenic heat production rate is closely linked to lithology. Generally, carbonate rocks have lower radiogenic heat production rates than clastic rocks, while basement metamorphic rocks exhibit intermediate values [5]. However, even within the same lithology, there can be significant variation, particularly in limestone and dolomite. Figure 5 shows the triangular diagram illustrating the contributions of U, Th, and K elements to the heat production of rock samples. A total of 6572 data points from 26 wells were analyzed. As depicted in Fig. 5, the contribution of Th to heat production is higher in terrigenous sedimentary rocks such as sandstone, mudstone, and siltstone compared to carbonate rocks. Group A, mainly consisting of metamorphic rocks and some sandstone and mudstone, shows Th contributing over 50% to heat production, while the contributions of K and U are relatively low. Group B, predominantly composed of siltstone, sandstone, and mudstone, shows U contributing more than 80%, with K ranging from 40 to 70%. Carbonate rocks, including dolomite and limestone, are predominantly found in Area C, where uranium (U) contributes the most

**Table 2** Radiogenic heat production rates in different formations of typical Wells in eastern Ordos Basin

| Layer | J06 | J05 | Y63 | T116 | T90 | S147 | Y06 | M46 | Y42 | M59 |
|---|---|---|---|---|---|---|---|---|---|---|
| Q-T Depth/m | 2376–2574.5 | 2475.1–2570.1 | 2003.7–2198.8 | 2291.6–2404.1 | 2234.3–2369.3 | 1899.6–2030.9 | 1488.9–1646.4 | 1323.75–1455 | 1414.8–1583.5 | 1560.9–1680.9 |
| A/μW·m$^{-3}$ | 1.547 | 1.54 | 1.436 | 1.528 | 1.587 | 1.515 | 1.318 | 1.589 | 1.441 | 1.603 |
| $P_2$sh Depth/m | 2574.5–2820.4 | 2570.1–2870.1 | 2198.7–2438.8 | 2404.1–2666.6 | 2369.3–2676.8 | 2030.9–2330.9 | 1646.4–1878.9 | 1455–1755 | 1583.5–1846 | 1680.9–1958.4 |
| A/μW·m$^{-3}$ | 1.56 | 1.51 | 1.6008 | 1.518 | 1.665 | 1.338 | 1.856 | 1.515 | 2.258 | 1.817 |
| $P_2$s Depth/m | 2820.4–2953.3 | 2870.1–3007.6 | 2438.8–2555 | 2666.6–2794.1 | 2676.8–2785.5 | 2330.9–2458.4 | 1882.6–2017.6 | 1755–1897.5 | 1846–1996 | 1958.4–2085.9 |
| A/μW·m$^{-3}$ | 1.317 | 1.88 | 1.704 | 1.97 | 1.81 | 1.462 | 1.343 | 1.723 | 2.015 | 2.108 |
| $P_1$x Depth/m | 2953.3–3125.8 | 3007.6–3175.1 | 2555–2697.5 | 2794.1–2921.6 | 2785.5–2928 | 2458.4–2634.6 | 2017.6–2160.1 | 1897.5–2062.5 | 1996–2153.5 | 2085.9–2247.1 |
| A/μW·m$^{-3}$ | 1.69 | 1.87 | 1.698 | 1.763 | 1.913 | 1.534 | 1.523 | 1.842 | 2.085 | 2.013 |
| $P_1$s Depth/m | 3125.8–3242 | 3175.1–3267.6 | 2697.5–2787.5 | 2921.6–3026.6 | 2928–3014.3 | 2634.6–2739.6 | 2160.1–2238.9 | 2062.5–2171.25 | 2153.5–2262.3 | 2247.1–2355.9 |
| A/μW·m$^{-3}$ | 1.90 | 2.45 | 2.007 | 2.24 | 2.211 | 2.3 | 2.267 | 2.227 | 2.198 | 2.849 |
| $C_3$t Depth/m | 3242–3279.5 | 3267.6–3307.6 | 2787.5–2832.5 | 3026.6–3052.9 | 3014.3–3040.5 | 2739.6–2777.1 | 2238.9–2268.9 | 2171.25–2227.5 | 2262.3–2292.3 | 2355.9–2400.9 |
| A/μW·m$^{-3}$ | 2.5 | 1.295 | 1.044 | 2.52 | 2.777 | 1.654 | 3.093 | 1.59 | 2.023 | 1.857 |
| $C_2$b Depth/m | 3279.5–3324.5 | 3307.6–3355.1 | 2832.5–2847.5 | 3052.9–3064.1 | 3040.5–3051.8 | 2777.1–2822.1 | | 2231.3–2276.3 | 2292.3–2326 | 2400.9–2457.1 |
| A/μW·m$^{-3}$ | 1.48 | 2.322 | 2.6 | 1.702 | 2.459 | 1.93 | | 2.172 | 3.378 | 3.871 |
| O Depth/m | 3324.5–3965.8 | 3355.1–3722.6 | 2847.5–3230 | 3064.1–3461.6 | 3051.8–3426.8 | 2822.1–3245.9 | 2268.9–2658.9 | 2276.3–2396.3 | 2326–2408.5 | 2457.1–2584.6 |
| A/μW·m$^{-3}$ | 0.69 | 0.562 | 0.715 | 0.589 | 0.582 | 0.511 | 0.874 | 0.768 | 1.428 | 1.084 |
| Є Depth/m | | | 3230–3365 | | | | | | | |
| A/μW·m$^{-3}$ | | | 0.968 | | | | | | | |
| Base Depth/m | 3965.8–3980.8 | | 3601.3–3642.5 | | | | | | | |
| A/μW·m$^{-3}$ | 0.41 | | 0.837 | | | | | | | |

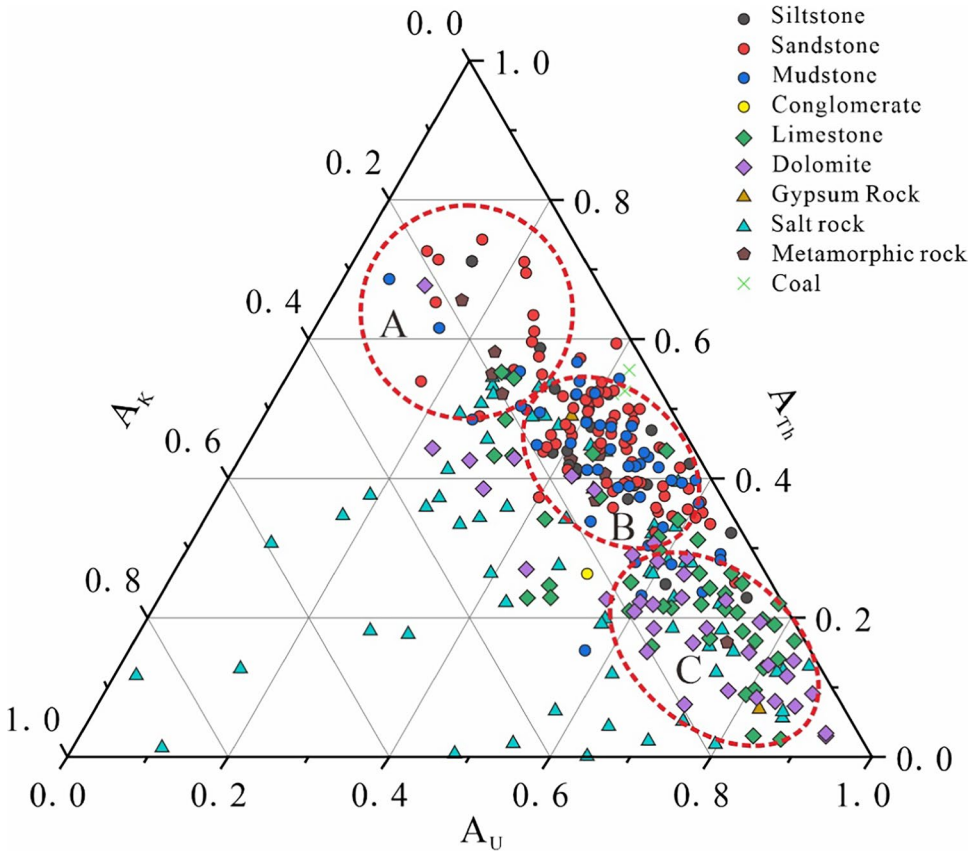


**Fig. 5** Contribution of U, Th, and K to radioactive heat rates in rock samples

(typically over 80%) and thorium (Th) contributes the least (usually less than 30%). Salt rocks are extensively distributed, with some samples exhibiting Th contributions as low as 1%, while potassium (K) can contribute up to 85%. The vertical distribution of uranium (U), thorium (Th), and potassium (K), along with their element ratios (U/K, U/Th, and Th/K), provides insights into the sedimentary environment and its history [27–29]. Uranium, being highly soluble and mobile, migrates easily, while thorium lacks these characteristics [30]. Consequently, the Th/U ratio serves as an indicator of the paleoenvironment's redox conditions. In an oxidizing environment, the Th/U ratio is typically greater than 6, while in a reducing environment, it is less than 2. Potassium, due to its activity, does not readily accumulate in sediments; hence, its concentration in sedimentary rocks is often linked to the clay mineral and K-mineral content in the source area [31]. Potassium content tends to be higher in shallow, near-shore waters, and lower in the open sea. Therefore, the Th/K ratio can reflect changes in water depth [32], with long-weathered sediments having a Th/K ratio greater than 7, and deep-water, low-energy environments showing relatively low Th/K values [33]. As shown in Fig. 6, the Th/U ratio of clastic rocks in the eastern Ordos Basin generally falls between 1 and 6, while the Th/U ratio of metamorphic rocks is typically greater than 6. The Th and U contents in salt rocks and some dolomites are relatively low, resulting in a lower overall radiogenic heat production rate. The Th/U ratio of marine sedimentary rocks, including clastic rocks deposited in shallow, oxygen-rich environments and carbonate rocks from deep, reducing conditions, decreases progressively from sandstone to siltstone, mudstone, and finally dolomite. In continental sedimentary rocks, the Th/U ratio of mudstone and siltstone lies in the intermediate range, while sandstone exhibits the greatest variability, indicating that grain size changes in continental sediments reflect differing sedimentary processes. The variation in Th and U also mirrors the influence of different sedimentary environments on their distribution. The average radiogenic heat production rates of U, Th, and K in various lithologies, along with their contributions to the total heat generation, are summarized in Table 3. The average radiogenic heat production rates for different rock types are as follows (in $\mu W/m^3$): sandstone ($1.68 \pm 0.41$), siltstone ($1.55 \pm 0.66$), mudstone ($2.05 \pm 0.70$), limestone ($0.51 \pm 0.48$), gypsum ($0.55 \pm 0.30$), salt rock ($0.27 \pm 0.18$), dolomite ($0.40 \pm 0.26$), metamorphic rock ($2.01 \pm 0.79$), and coal ($1.06 \pm 0.71$). In continental sedimentary rocks, the heat production contributions of U, Th, and K are 42–47%, 42–53%, and 5–11%, respectively. In marine carbonate rocks, uranium is the dominant heat producer, contributing approximately 65.5% on average, with some samples showing a contribution as high as 93%. For evaporitic rocks like salt and gypsum, U, Th, and K contribute

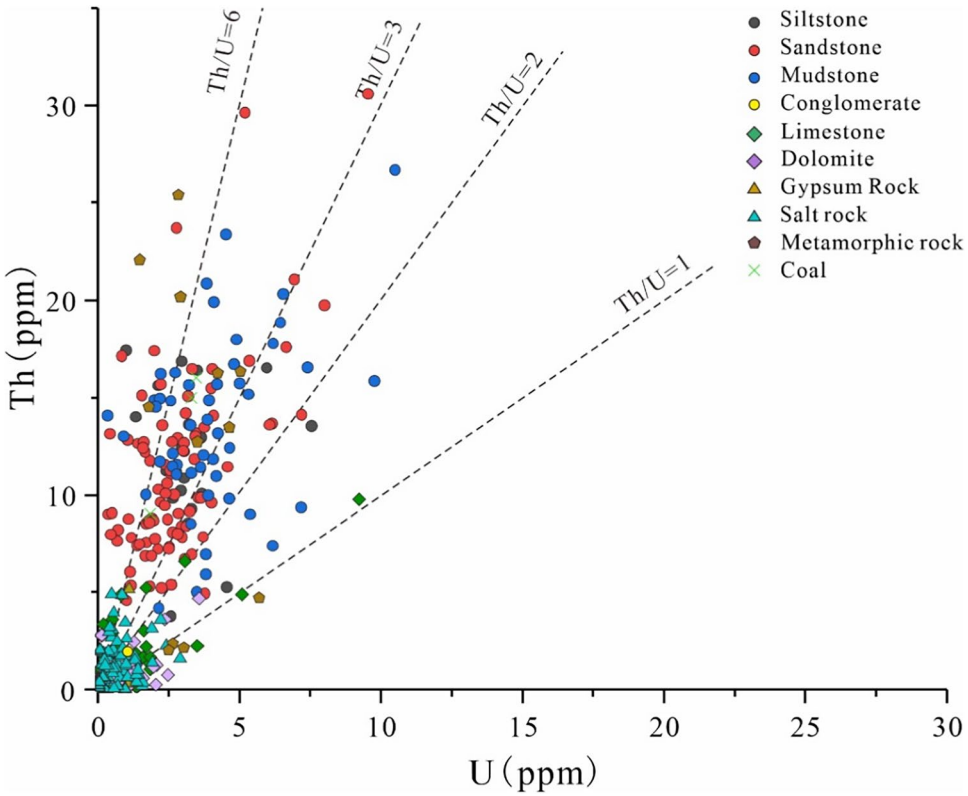


**Fig. 6** Relationship Between Th and U in Various Rock Samples

**Table 3** Average radiogenic heat production rates of radioactive elements in different lithologies and their contribution to rock heat production

| Lithology | N | $A_U$ | (%) | $A_{Th}$ | (%) | $A_K$ | (%) | A |
|---|---|---|---|---|---|---|---|---|
| Siltstone | 20 | 0.74 ± 0.32 | 44 | 0.76 ± 0.25 | 45 | 0.18 ± 0.09 | 11 | 1.68 ± 0.41 |
| Sandstone | 90 | 0.67 ± 0.41 | 43 | 0.73 ± 0.31 | 47 | 0.15 ± 0.07 | 10 | 1.55 ± 0.66 |
| Shale | 50 | 0.97 ± 0.51 | 47 | 0.87 ± 0.32 | 42 | 0.21 ± 0.09 | 10 | 2.05 ± 0.70 |
| Limestone | 47 | 0.32 ± 0.38 | 64 | 0.13 ± 0.12 | 26 | 0.05 ± 0.04 | 10 | 0.51 ± 0.48 |
| Dolomite | 36 | 0.27 ± 0.21 | 67 | 0.08 ± 0.07 | 21 | 0.05 ± 0.03 | 12 | 0.40 ± 0.26 |
| Gypsum | 2 | 0.29 ± 0.01 | 52 | 0.20 ± 0.24 | 36 | 0.07 ± 0.04 | 12 | 0.55 ± 0.30 |
| Rock Salt | 70 | 0.13 ± 0.12 | 49 | 0.07 ± 0.07 | 27 | 0.06 ± 0.07 | 38 | 0.27 ± 0.18 |
| Coal | 3 | 0.45 ± 0.30 | 42 | 0.56 ± 0.36 | 53 | 0.05 ± 0.05 | 5 | 1.06 ± 0.71 |
| Metamorphic Rock | 12 | 0.85 ± 0.33 | 42 | 0.87 ± 0.56 | 43 | 0.29 ± 0.19 | 15 | 2.01 ± 0.79 |

50.5%, 31.5%, and 11%, respectively. In metamorphic rocks, the heat production contributions of U and Th are similar, while K contributes less to the overall heat production.

In summary, the radiogenic heat production rate of rocks in the eastern Ordos Basin is relatively low compared to those in the East China Basin and Qaidam Basin. The average radiogenic heat production rate of rock samples in this area is 1.489 ± 0.903 μW/m$^3$, which is below the global average and similar to the radiogenic heat production rate in the Junggar Basin (1.137 μW/m$^3$). This is likely due to the widespread presence of thick layers of dolomite, salt rock, and gypsum, which have low radiogenic heat production rates.

## The contribution of the sedimentary layer to terrestrial heat flow

Previous studies have shown that the Earth's heat flow in the Ordos Basin ranges from 46 to 70 mW/m$^2$, with an average value of 62 mW/m$^2$, classifying it as a moderate-temperature basin [28]. Zhang Sheng [34] calculated the heat flow values for different tectonic units in the Ordos Basin, revealing an average heat flow of 62 mW/m$^2$ for the entire basin. Specifically, the Yishan Slope tectonic unit has an average heat flow of 65 mW/m$^2$, the Tianhuan Depression has an average of 58 mW/m$^2$, and the Weibei Uplift has an average of 65 mW/m$^2$. In this study, 56 class A heat flow data points were collected from the study area and its surroundings, along with 73 class B heat flow

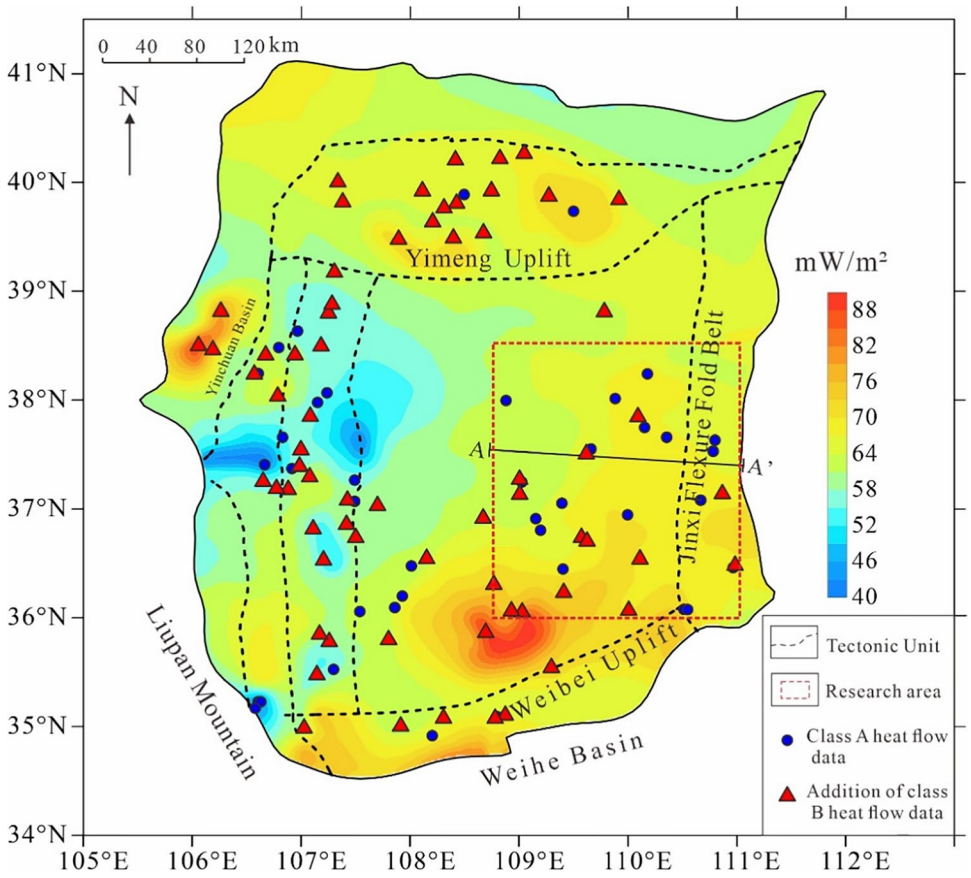


**Fig. 7** The distribution of terrestrial heat flow in the Ordos Basin and surrounding areas

data points obtained through steady-state temperature measurements, combined with thermal conductivity data. A distribution map of the Earth's heat flow in the study area and its vicinity was then constructed (Fig. 7). As shown in the map, the heat flow values in the Ordos Basin and surrounding regions range from 40 to 90 mW/m$^2$, with an average of 64 mW/m$^2$. The average heat flow in the western region is relatively low at 57 mW/m$^2$, while the eastern region shows a higher average of 68 mW/m$^2$. As seen in Figs. 7, 8, the variations in heat flow are closely aligned with the lithospheric structure. Specifically, the Moho surface depth increases gradually from east to west, and the heat flow also decreases progressively in the same direction.

The surface heat flow $q_0$ is composed of two components: the heat generated by radioactive decay in the crust ($q_c$), and the mantle heat flow ($q_m$). The relationship between these components is expressed as [35]:

$$q0 = qm + qc = qm + \sum_{i=1}^{n} Ai \cdot Zi \tag{3}$$

where $D$ is the characteristic depth of radioactive element enrichment (km), $n$ is the number of layers considered (km), and $A$, $A_i$ represents the raw radiogenic heat production rate (μW/m$^3$). Using a stratified crust model and the 'back stripping' method, heat flow values for different layers can be determined.

To evaluate the contribution of sedimentary layers to surface heat flow in the eastern Ordos Basin, the A–A′ profile in the study area is taken as a representative example. The sedimentary layer in the central Yishan slope exhibits the highest heat flow contribution, ranging from 3.95 to 5.05 mW/m$^2$, accounting for 5.01 to 8.28% of the total surface heat flow. In contrast, the sedimentary heat flow contribution in the Jinxi flexural belt is relatively low, with an average value of 0.80 mW/m$^2$, representing approximately 1.18% of the surface heat flow. The heat production of the sedimentary layer is generally higher in regions with a deeper basement compared to those with a shallower basement. In the flexural fold zone of western Shanxi, where the sedimentary cover is thin, the heat production rate of the sedimentary layer is relatively low. It is widely accepted that tectonic and magmatic activities lead to the concentration of radioactive thermogenic elements in the middle, lower, and upper crust [35, 36]. According to the data presented in Fig. 8, the heat production in the middle and lower crust of the region ranges from 10.02 to 10.91 mW/m$^2$, while the heat production in the basement varies from 11.06 to 12.04 mW/m$^2$ (the radiogenic heat production rates of the basement and middle-lower crust are derived from [37–40] in the calculations). As a result, the total crustal heat flow in this area is estimated to range from 23.09 to 26.13 mW/m$^2$. The average contribution of crustal heat flow in the middle and eastern sections of the Yishan slope is

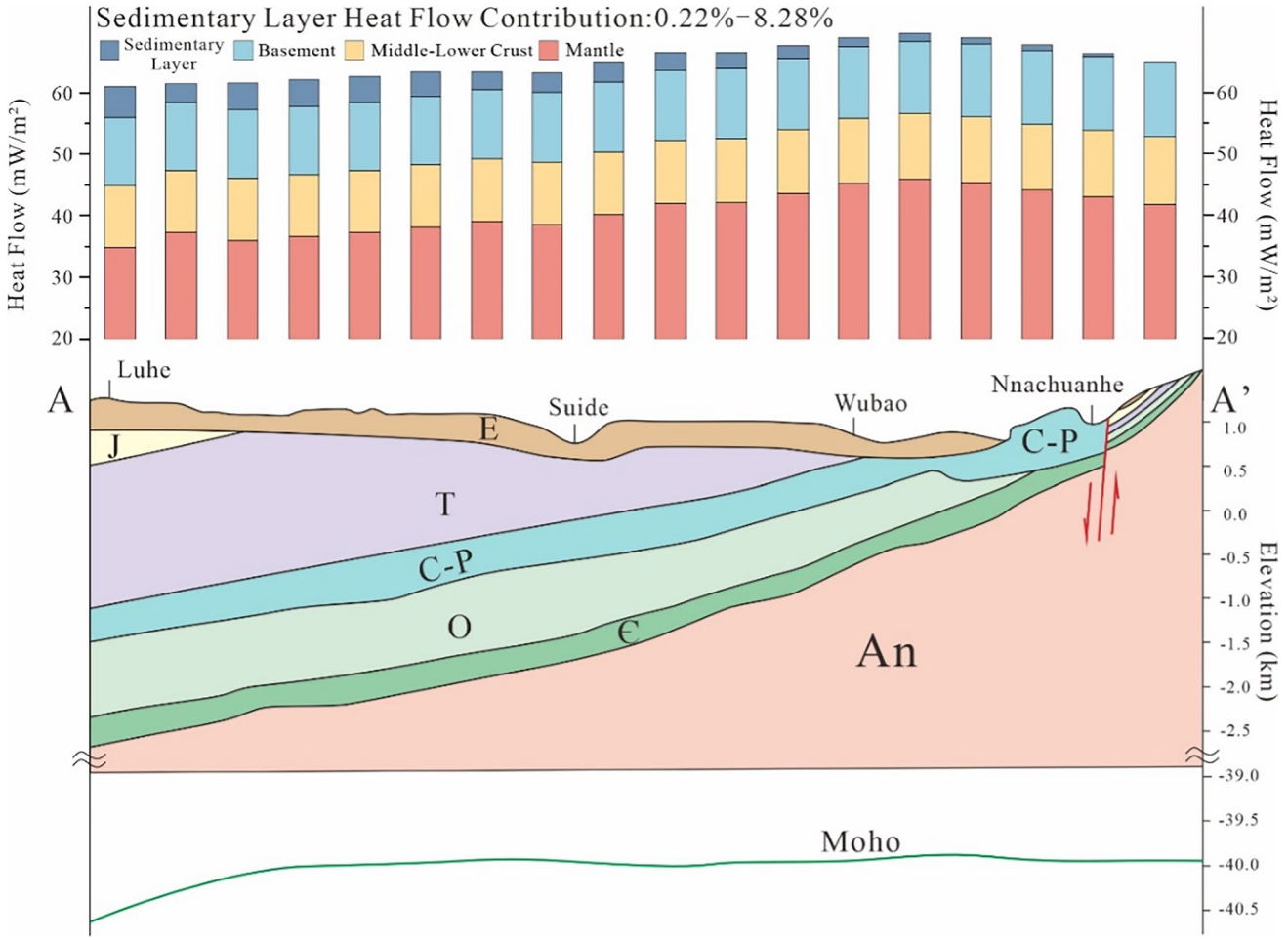


**Fig. 8** Contribution of heat production in the Eastern Ordos Basin Profile

approximately 40.85% of the total heat flow, while the contribution from the west Jinxi flexural belt averages around 34.71%. Therefore, surface heat flow in the eastern Ordos Basin is predominantly influenced by the distribution of mantle heat flow.

## Conclusions

Compared to measured values, the radiogenic heat production rate calculated using natural gamma spectrum logs is more accurate. The average radiogenic heat production rate in the study area is $1.489 \pm 0.903$ μW/m$^3$. Specifically, the average radiogenic heat production rates for sandstone, siltstone, and mudstone are $1.55 \pm 0.68$, $1.68 \pm 0.41$, and $2.05 \pm 0.7$ μW/m$^3$, respectively. In contrast, marine carbonate rocks exhibit lower radiogenic heat production rates, with limestone at $0.51 \pm 0.48$ μW/m$^3$ and dolomite at $0.40 \pm 0.26$ μW/m$^3$. The radiogenic heat production rates of salt rocks and gypsum are even lower, averaging $0.27 \pm 0.18$ μW/m$^3$. In the eastern Ordos Basin, the contributions of U, Th, and K to heat generation range from 42 to 67%, 21 to 53%, and 5 to 38%, respectively. Overall, uranium (U) makes the largest contribution, followed by thorium (Th) and potassium (K). The heat production of the sedimentary layer in this area ranges from 1.37 to 3.45 mW/m$^2$, accounting for 0.22 to 8.28% of the total surface heat flow. Therefore, surface heat flow in the eastern Ordos Basin is predominantly influenced by the distribution of mantle heat flow.

**Funding** The study was supported by the National Key Research and Development Program of China (Grant No. 2021YFA0716000) and the National Natural Science Foundation of China (Grant No. 42172334).

## Declarations

**Competing interests** The authors declare that they have no known competing financial interests or personal relationships that could have appeared to influence the work reported in this paper.

## References


1. Hurley PM, Fairbairn HW (1953) Radiation damage in Zircon. Geol Soc Am Bull 64(6):659
2. Joly J (2004) Radioactivity and Geology, an account of the influence of radioactive energy on rerrestrial history
3. Buntebarth G (1984) Geothermics: an introduction. Springer Verlag, New York
4. Qiu N, Shengbiao Hu, He L (2019) Geothermics in sedimentary basins. China University of Petroleum Press, China
5. Zhu C, Xu M, Qiu N, Hu SB (2018) Heat production of sedimentary rocks in the Sichuan basin, southwest China. Geochem J 52(5):401–413
6. Zhang L, Li X, Zhang S, Zhu GL, Xu WH, Feng QD, Deng ZH (2024) Deep-seated radiogenic heat production characteristics in the northeastern Gonghe basin (Northeastern Qinghai-Tibet plateau) from deep borehole samples: implications for the formation of hot dry rock resources. Geothermics 123:103110
7. Arevalo R, Mcdonough WF, Luong M (2009) The K/U ratio of the silicate Earth: Insights into mantle composition, structure and thermal evolution. Earth Planet Sci Lett 278(3):361–369
8. Zhang C, Hu SB, Song RC, Zou YH, Jiang GZ, Lei YD, Zhang SS, Wang ZT (2020) Genesis of the hot dry rock geothermal resources in the gonghe basin: constraints from the radiogenic heat production rate of rocks. Chin J Geophys 63(07):2697–2709
9. Brady R, Ducea M, Kidder S, Saleeby J (2006) The distribution of radiogenic heat production as a function of depth in the Sierra Nevada Batholith. California Lithos 86(3):229–244
10. Rybach L (1986) Amount and significance of radioactive heat sources in sediments
11. Luo M, Pan HP, Zhao YG et al (2008) Natural radioactivity logs and interpretation from the CCSD main hole. J Earth Sci 05:661–671
12. Qi K, Ren Z, Cui J, Yu Q (2020) Meso-Cenozoic lithospheric thermal structure and its significance in the evolution of the lithosphere in the Ordos Basin, WNCC, China. Int Geol Rev 63:2146–2165
13. Ren Z, Yu Q, Cui J et al (2017) Thermal evolution history of the Ordos Basin and its control on oil and gas. Earth Sci Front 24(03):137–148
14. Ren Z, Zhao Z (1997) Late Mesozoic comparative research on the geothermal field of the Ordos Basin and Qinshui Basin. Acta Sedimentol Sin 15(2):134–137
15. Li EX, Li YZ (2008) Tectonic evolution of the western margin of the Ordos Basin (Central China). Russ Geol Geophys 49(1):23–27
16. Wang S, Li D, Li J, Đồng Đ, Zhang W, Ma J (2011) Exploration potential of shale gas in the Ordos Basin. Nat Gas Ind 31:40–46
17. Shen Y, Qin Y, Wang GG, Guo YH, Shen J, Gu JY, Xiao Q, Zhang T, Zhang CL, Tong GC (2017) Sedimentary control on the formation of a multi-superimposed gas system in the development of key layers in the sequence framework. Mar Pet Geol 88:268–281
18. Chen Y, Wang Y, Guo M, Wu HY, Li J, Wu WT, Zhao JZ (2020) Differential enrichment mechanism of organic matters in the marine-continental transitional shale in northeastern Ordos Basin, China: control of sedimentary environments. J Nat Gas Sci Eng 83:103625
19. Ma DY, Chen YH, Wang YB, Guo MQ, Qu L, Zhao JZ, Wu HY (2021) Sealing capability evaluation of the upper Paleozoic cap rock in the Eastern Ordos Basin. Nat Gas Geosci 32(11):1673–1684
20. Liu C, Lei M, Sun B, Wang X (2023) Origin and process of carbon isotopic reversal of tight sandstone gas in the Shixi gas field, eastern margin of Ordos Basin. Int J Coal Geol 276:104327
21. Orozova-bekkevold I (2024) In-situ radiogenic heat production in the Cenozoic sediments of the North sea. Phys Chem Earth Parts A/B/C 135:103602
22. He LJ, Hu SB, Yang WC, Wang JY (2009) Radiogenic heat production in the lithosphere of Sulu ultrahigh-pressure metamorphic belt. Earth Planet Sci Lett 277(3):525–538
23. Rybach L (1976) Radioactive heat production in rocks and its relation to other petrophysical parameters. Pure Appl Geophys 114(2):309–317
24. Ding C (2010) Study on the thermal evolution history and natural gas accumulation timing in the Northeastern Ordos Basin. Northwest University, Evanston
25. Ren ZL, Zhang S, Gao SL, Cui JP, Xiao YY, Xiao H (2007) Tectonic thermal evolution history of the Ordos basin and its implications for Reservoir and Ore formation. J Earth Sci S1:23–32
26. Sun SH, Liu SS, Wang J (1996) Heat flow field characteristics of the Ordos Basin. Geotecton Metallog 01:29–37
27. Qi K (2018) Preliminary study on the meso-cenozoic thermal regime and lithospheric dynamic evolution of the Ordos Basin. Northwest University, Evanston
28. Abbady AG (2010) Evaluation of heat generation by radioactive decay of sedimentary rocks in Eastern Desert and Nile Valley, Egypt. Appl Radiat Isot 68(10):2020–2024
29. Ribeiro FB, Roque A (2001) Vertical distributions of uranium, thorium and potassium and of volumetric heat production rates in the sediments of the São Francisco Basin, Central Brazil. Appl Radiat Isot 55(3):393–405
30. Mclennan SM, Taylor SR (1980) Th and U in sedimentary rocks: crustal evolution and sedimentary recycling. Nature 285(5767):621–624
31. Fu X, Li X, Zhu C, Su YX, Cui KN, Meng Q (2024) Rock heat production and its contribution to terrestrial heat flow in the Northern Songliao Basin, Northeast China. J Radioanal Nucl Chem 333(8):3751–3765
32. Čermák V (1982) Crustal temperature and mantle heat flow in Europe. Tectonophysics 83(1):123–142
33. Zhang S (2006) Study on the Paleo-Temperature evolution and its relationship with various energy and mineral resources in the Ordos Basin. Northwest University, Evanston
34. Roy RF, Blackwell DD, Birch F (1968) Heat generation of plutonic rocks and continental heat flow provinces. Earth Planet Sci Lett 5:1–12
35. Newton RC (1986) Fluids of granulite facies metamorphism. Springer, New York
36. Wang Y, Wang J, Deng J (2001) Heat flow constraint on the abundance of uranium, thorium and potassium in crust and lithosphere of the continental area of China. Prog Geophys 16:21–30
37. Wang GL, Liu F, Lin WJ, Zhang W, Yuan RX, Xi YF, Wei SC, Liao YZ, Wang YR (2023) The crustal heat production rate and crustal and mantle heat flow distribution in the land areas of China. Chin J Geophys 66(12):5041–5056
38. Yan MC, Chi QH (1997) Chemical composition of the crust and rocks in eastern China. Science Press, Beijing
39. Lin Y (2010) Deep crustal rock composition and element abundance in Central inner Mongolia. China University of Geosciences, Beijing
40. Chen HD, Li J, Jing YZ, Lu N, Zhang GZ (2014) Zircon U-Pb ages and geological significance of Zisu Schist Granulite in Liangcheng Area, Central inner Mongolia. Geol China 41(4):1136–1142